Heterogeneity and Dynamics in Azobenzene Methacrylate Random and Block Copolymers: A Nanometer-Nanosecond Study via Electron Spin Resonance Spectroscopy

L. Andreozzi,*[,†] M. Giordano,[†] G. Galli,[‡] E. Martinelli,[‡] F. Zulli[†]

[†]Department of Physics "E. Fermi", University of Pisa and IPCF-CNR, Pisa, Italy

[‡]Department of Chemistry and Industrial Chemistry, University of Pisa, and INSTM, Pisa, Italy

AUTHOR INFORMATION

Corresponding Author

*E-mail: laura.andreozzi@df.unipi.it (L.A.).

Notes

The authors declare no competing financial interest.

ABSTRACT: The effects of the different architecture on the dynamic response at nanometers and nanoseconds was investigated by means of electron spin resonance spectroscopy in a series of random and block copolymers of an azobenzene methacrylate (MA4) and methyl methacrylate (MMA) counits. The study evidenced the presence of fast and slow molecular sites for the molecular reorientation at nanoscale, modulated by the amount of MA4 counits in the random copolymers, and by the self-assembly in supramolecular structures in the block copolymers. A series of dynamics features was found, such as the presence of memory effects, the existence and the degree of coupling of the rotational dynamics to the structural relaxation of the matrix or to its viscosity, and the population of the different dynamic sites, that provided a detailed description and characterization of the different mechanisms leading the dynamic response of the structurally different copolymer systems.

1. INTRODUCTION

Since the first report on the photo-addressed digital and holographic optical storage on liquid crystalline azobenzene polymers,[1] significant progress in the fundamental understanding and applied science of photo-addressing diverse chemical and physical effects has continually been achieved for such type of functional polymers.[2] The azobenzene chromophore acts as both a photo-responsive moiety and a mesogenic group. Due to its repeated *trans-cis-trans* cycles within a polymer matrix reversible processes of photo-orientation, photo-selection, and photo-modulation can be generated from the molecular level over several spatial and temporal length scales in a variety of materials.[3] In our own work we have shown that nematic azobenzene methacrylate polymers are suitable candidates for all-optical reversible information data storage at both micrometer and nanometer length scales.[4,5]

Whilst early investigations concentrated on azobenzene homopolymers, it soon became apparent that the more complex structures and architectures of copolymers may be exploited to effectively tailor photo-addressed chemical and physical processes.[3] On the one hand, random copolymers are matrix materials where excessive steric crowding of azobenzene counits along the polymer backbone may be remediated by dilution with different, not necessarily mesogenic, counits resulting in more finely tuned responses. On the other hand, block copolymers may provide highly localized optical media upon microphase separation, when the mesogenic azobenzene block is confined in submicron- or nano-scale domains dispersed in the amorphous phase of the non mesogenic block matrix. Thus, there is a still growing interest in such materials for application in various technological fields, namely optical nanodata storage.

The possibility of achieving an effective high-resolution and long-term data storage deals with crucial parameters such as bit stability, homogeneity at molecular level, and working temperature.[6,7] Therefore, a full knowledge of the polymer characteristics should be gained by different spectroscopic techniques that cover several length and time scales. Accordingly,

calorimetry and rheology can be adopted to investigate thermal properties of the melt and dynamics of polymer chains,[8−10] while electron spin resonance (ESR) spectroscopy can be employed to study the stability of different molecular sites and their correlation times as a function of temperature and to reveal connections between nanoscale dynamics with chain dynamics and thermal responses of the melt.[11]

It is known that ESR spectroscopy is a powerful technique to investigate molecular dynamics in simple and complex liquids, having proved to be very sensitive to details of the molecular rotation and to the structure of the matrix of both simple and complex liquids of medium to high viscosity.[12,13] ESR studies in diamagnetic systems are often carried out by dissolving very small quantities of paramagnetic molecular tracers, so called spin probes,[12] whose size and shape select the length scale of the experiment. The cholestane spin probe was profitably employed in literature to study reorientation dynamics including liquid crystal polymers.[7,11,14−22] It locates length and time scales at the nanometers and nanoseconds, characteristic of cooperative processes. Therefore, this could play a fundamental role in evidencing possible discrepancies of the global melt dynamics because of specific local chain properties. So, by means of ESR spectroscopy it was possible to reveal dynamics crossovers in polymers and soft matter[16,17] and decoupling from the macroscopic overall dynamics of the matrix and its dynamics at nanoseconds. Heterogeneity was also found at the nanoscale in polymers.[7,23] A further main finding in ESR studies of paramagnetic molecular tracers in polymers is the sensitivity to cooperative dynamics of the polymer matrix associated with signatures and dynamic anomalies in the temperature dependence of the times of the molecular reorientation.[19−22,24]

The present work reports on an ESR investigation, complemented by rheology and calorimetry studies, into the dynamics and matrix heterogeneity of MA4-MMA random and diblock copolymers (Figure 1). We highlight how the different architecture results in very different dynamic responses and matrix heterogeneities.

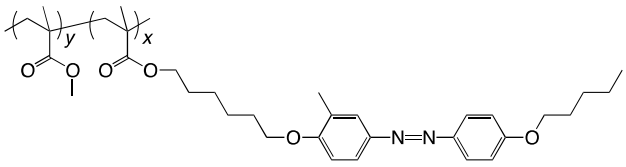

Figure 1. General sketch of the polymer samples investigated with their mole fraction: PMA4 homopolymer (*x*=100 mol%), PMMA homopolymer (*y*=100 mol%), random copolymers R*x* (*x*=90, 80, 10 mol%, *y*=100–*x*), and block copolymers B*x* (*x*=20, 10, 3 mol%).

2. EXPERIMENTAL SECTION

2.1. Polymers.

The random and diblock copolymers of the azobenzene methacrylate (MA4) with methyl methacrylate (MMA) (Table 1, Figure 1) were prepared by reported procedures.[4,25] In particular, the block copolymers were prepared by a sequence of two atom transfer radical polymerization (ATRP) steps, by which a PMMA macroinitiator block (Table 1, average degree of polymerization 200) was first formed and then used to incorporate the second MA4 block, so that polymers with well defined structure and low molar mass dispersion were obtained. The composition of the copolymers was determined from the integrated areas of the ^{1}H NMR well resolved signals of the $COOCH_3$ protons of the MMA counits (at 3.6 ppm) and the OCH_2 protons of the MA4 counits (at 3.9–4.1 ppm). Morphology was studied by AFM spectroscopy and discussed in a previous work.[4]

A conventional nomenclature was adopted in order to refer to random and block copolymers, R*x* and B*x*, respectively, where the index *x* indicates the mole fraction of MA4 counits in the copolymer.

2.2. Molar Mass Distribution and Thermal Characterization.

Average molar masses and molar mass distributions (Table 1) were determined by size-

exclusion chromatography (SEC) of chloroform solutions with a Waters 590 chromatograph, equipped with two Shodex KF804 columns, and both Waters R401 differential refractive index and PerkinElmer LC75 ultraviolet detectors, or by SEC of chloroform and tetrahydrofuran solutions with a JASCO PU-1580-CO2 chromatograph, equipped with two PLgel 0.005 mm MIXED-C and MIXED-D columns and both JASCO 830-RI differential refractive index and PerkinElmer LC75 ultraviolet detectors. Standard samples of polystyrene (molar mass 1–500 kg mol^{-1}) were used for calibration. Based on previous measurements,[26] we estimate that the absolute values of the molar masses in the distribution of these copolymer samples may differ by 10% from the respective SEC values.

Table 1. Chemical and Physical Characterization of the Copolymers

sample	x (mol%)	M_n (kg mol^{-1})	M_w (kg mol^{-1})	M_w/M_n	T_g^{PMA4} (K) [a]	T_g^{PMMA} (K)	T_{ni} (K)	T_{odt} (K)
PMMA	---	21	27	1.27	---	378	---	---
R90	90	53	180	3.61	306	---	353	---
R80	80	49	177	3.40	308	---	352	---
R10	10	22	57	2.62	356	---	---	---
B20	20	34	44	1.31	324	394	358	413
B10	10	27	34	1.27	328	397	353	423
B03	3	29	36	1.24	---	392	353	433

[a] Random copolymers showed one glass transition reported as T_g^{PMA4}.

Differential scanning calorimetry (DSC) measurements of random copolymers were carried out with a Perkin-Elmer DSC7 calorimeter, recording thermograms on heating at 10 K min^{-1} after cooling at 40 K min^{-1} from about 383 K. The DSC curves of block copolymers were recorded with a Mettler Toledo DSC30 calorimeter on heating from about 225 K at 10 K min^{-1} after cooling at 20 K min^{-1} from about 473 K.

All copolymers, except R10, were liquid crystalline and a nematic-to-isotropic transition

temperature T_{ni} was found. The weakening of the nematic potential as the content of MA4 counits decreased in random copolymers ultimately led to disappearance of the nematic phase in R10. Random copolymers presented one glass transition temperature T_g, while block copolymers, except B03, exhibited two T_gs: T_g^{PMMA} and T_g^{PMA4}. This is expected of microphase separated block copolymers.[27]

The T_g and T_{ni} transition temperatures were determined by using different definitions. For random copolymers, the glass transition at T_g was determined according to the enthalpic definition.[28] For block copolymers, the T_g^{PMMA} and the T_g^{PMA4} were measured following the inflection method[29] due to the broadened shape of the DSC thermograms at lower temperatures. The nematic-to-isotropic transition temperature T_{ni} was measured with the peak definition.

Previous investigations in block copolymers by means of atomic force microscopy showed that the block copolymers were microphase separated up to an order-to-disorder transition temperature (T_{odt}), above which one disordered phase existed.[4]

The transition temperatures are reported in Table 1.

2.3. Rheological Characterization.

Rheological measurements for random copolymers were carried out with a Haake RheoStress RS150H rheometer equipped with a TC501 temperature control system and parallel-plate sensor system (20 mm diameter) at temperatures ranging from roughly T_g up to T_g+120 K. The viscoelastic characterization of block copolymers was carried out with an Anton Paar Physica MCR301 rheometer by means of a plane-plate sensor system (25 mm diameter), from temperatures at about T_g^{PMMA} for B03 or 30–40 K above T_g^{PMA4} for B10 and B20 up to temperatures in the flow region. A CTD450 temperature control unit kept the temperature of the sample stable within 0.1 K. In all cases, oscillatory, steady-state viscosity and creep-recovery experiments were performed. All the measurements were gap-independent. The applied stress intensities were chosen to perform

measurements in the linear viscoelastic regime response, as verified by suitable tests on the polymer matrices of interest.

Steady-state viscosity, creep and creep-recovery experiments were carried out in order to evaluate zero-shear viscosity. In the case of creep-recovery experiments, the viscosity of the materials was evaluated without breaking the linear viscoelastic limit.[26,30–32] In oscillatory experiments, isothermal frequency sweeps were usually performed in the range from 10^{-3} Hz to 24.4 Hz. However, on approaching T_g, the lower limit was extended down to 10^{-4} Hz. From oscillatory experiments, zero-shear viscosity was obtained according to the relationship $\eta=\lim_{\omega\to 0} G''/\omega$,[30,33] whenever possible. G'' is the loss modulus, which is defined, together with the shear modulus G', in terms of the complex modulus G^* as $G^*=G'+iG''$, with $i^2=-1$.

2.4. ESR: Apparatus and Experimental Techniques.

ESR measurements were carried out with a continuous wave Bruker ER200D-SRC spectrometer operating in the X-band, equipped with an X band bridge (Bruker ER042-MRH) and a NMR gaussmeter ER035M. The temperature was controlled with a gas-flow variable temperature unit (Bruker BVT100) with nominal accuracy of ±0.1 K. For more details about the procedure and the technique see Ref. 19 and references therein.

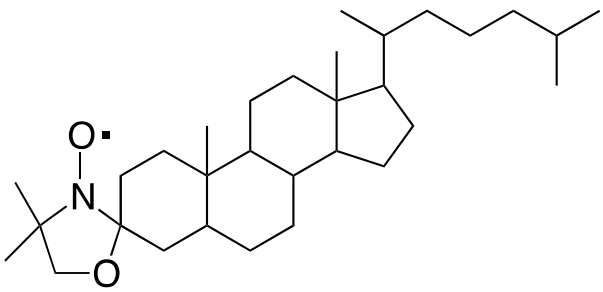

Figure 2. Structure of the cholestane spin probe.

The molecular tracer used in the present study is the cholestane nitroxide (3β-doxyl-5α-

cholestane, 98%, Aldrich, Figure 2), chosen because of its geometry and its good thermal stability.[12] The cholestane molecule is quite asymmetric in shape and can be sketched as a prolate ellipsoid with semiaxes of about 0.99 and 0.29 nm.[16,34] Its size is just across the nanometer length-scale that[7,21,22] characterizes the dynamic heterogeneity and cooperativity in polymers and supercooled liquids on approaching the glass transition. The cholestane rotational dynamics is described in terms of the diffusion model under cylindrical symmetry.[20,35,36] Accordingly, a spinning diffusion coefficient $D_{\|}$ characterizes the rotation along the symmetry axis of the molecule and a tumbling diffusion coefficient $D_{\perp}$ accounts for the rotation of the axis itself.[37] The ratio $D_{\|}/D_{\perp}$ resulted to be close to 15 for cholestane in all the investigated samples. For comparison purposes with the results of rotational dynamics reported in literature,[7,11,15] in this work the reorientation of cholestane is discussed in terms of a spinning correlation time, defined as $\tau_{\|}=1/(6D_{\|})$.[38]

The values of the principal components of the magnetic tensors were drawn by the ESR lineshape in a ultraslow motion regime,[39] according to a procedure detailed elsewhere.[35] The values of the Zeeman and hyperfine tensors in the molecular frame[12] are reported in Table 2.

Table 2. Values of the Magnetic Tensor Components in the Molecular Frame

samples	g_{xx}	g_{yy}	g_{zz}	a_{xx} (gauss)	a_{yy} (gauss)	a_{zz} (gauss)
R90, R80	2.0026	2.0092	2.0069	32.6	5.5	5.0
R10	2.0026	2.0093	2.0066	32.9	6.0	5.0
B20, B10, B03	2.0026	2.0092	2.0069	32.9	5.5	5.0

All the samples were prepared at room temperature by mixing two chloroform solutions containing predetermined amounts of polymer and cholestane, respectively. The resulting solutions had a concentration of about 10^{-3} cholestane/repeat unit molar ratio. The samples were then evaporated to complete dryness by heating under vacuum at a proper temperature, and finally sealed in a standard ESR tube.

Previous studies[7,11,15] on PMA4 homopolymers and random copolymers had evidenced the

presence of memory effects, because of the polymer thermal history, that affected the stability of the ESR lineshape. Therefore, to obtain stable and reproducible responses we followed a thermal procedure[7,15] involving the annealing of the sample in the isotropic phase at a temperature T_a, until a stable ESR spectrum was recorded. The samples were then cooled, and ESR spectra were recorded over sets of decreasing temperatures. Spectra in the upper temperature region were simply recorded on slowly heating the sample from T_a. No memory effects were detected in ESR lineshapes of the block copolymers and the spectra were just recorded at the desired temperature.

3. RESULTS AND DISCUSSION

3.1. Viscosity of Copolymers.

Rheological material functions, such as zero-shear viscosity η and complex shear modulus G^*, were investigated for random and block copolymers, from roughly T_g up to high temperatures, above T_{ni} and T_{odt}. The curves of zero-shear viscosity versus temperature, obtained from steady-state viscosity (for random copolymers only), creep-recovery and dynamics experiments, are shown in Figure 3. Values for selected literature PMMA homopolymers are also shown in Figure 3 for comparison.[40,41] No discontinuity was observed in the investigated temperature range for any sample, not even across T_{ni} or T_{odt}.[9,26,32]

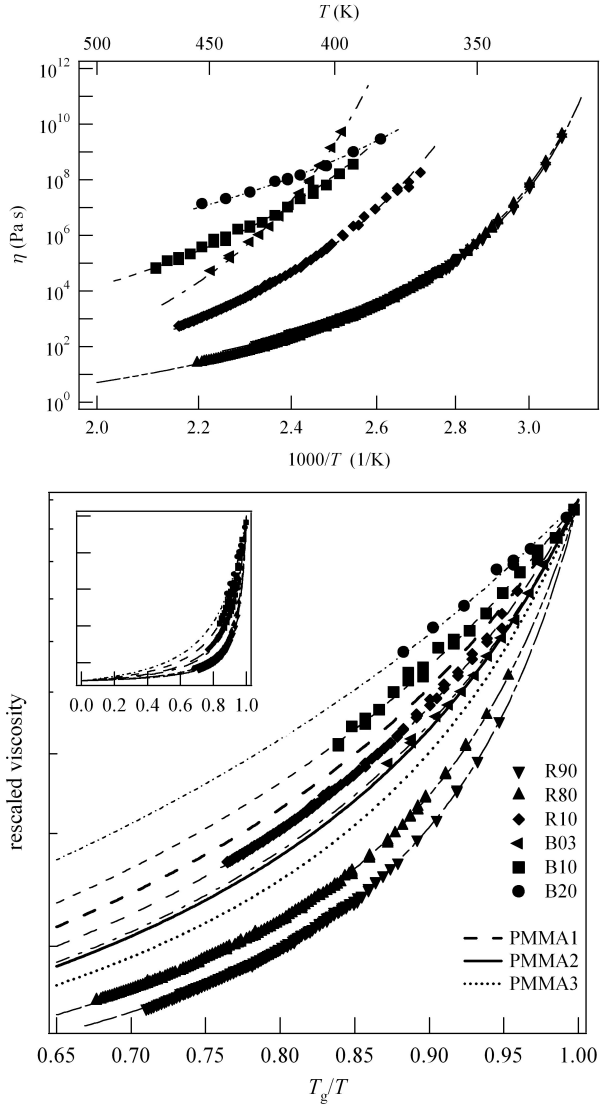

Figure 3. Top: viscosity of PMA4 copolymers as a function of 1000/T. Bottom: logarithm of the rescaled viscosity $(\eta(T)/\eta(T_g))(T_g-T_0)/T_b$ of PMA4 copolymers as a function of T_g/T; the rescaled viscosity of selected literature PMMA homopolymers[40,41] (Table 3) is also shown.

Moreover, the shear moduli in dynamic experiments carried out in the linear response regime did not show any heterogeneous behavior across the characteristic temperatures of the different samples.[26,32] However, the different chemical and structural arrangement of the block copolymers led to the failure of the time-temperature superposition[42] principle (TTS) in B20 and B10. Therefore, viscosity was only evaluated by creep-recovery experiments for these copolymers.[43] Interestingly enough, for B20 and B10, it was possible to collapse to a single master

curve the G' component of the shear modulus, by superimposing the isothermal frequency sweeps. This could be ascribed to the blocky nature of the copolymers for which the different temperature dependence of the monomeric friction coefficients of the counits affects to a greater extent the viscous properties rather than the elastic ones.[32]

For each sample of Figure 3, the viscosity temperature dependence can be profitably fitted by a single Vogel–Fulcher (VF) law[44]

$$\eta(T) = \eta_\infty \exp\left(\frac{T_b}{T - T_0}\right) \tag{1}$$

where T_b is the pseudo-activation temperature and T_0 is the Vogel temperature. The best fits are superimposed to the experimental curves in Figure 3. Values of T_b and T_0 are given in Table 3, where values[26] of η_∞ are also reported for the sake of completeness. In Table 3, the fitting parameters according to a VF dependence are also reported for the shift factor[45] $a(T)$ of G' in B20 and B10. The presence of different mechanisms driving elastic and viscous behaviors in these block copolymers is confirmed by the non coincident values of the VF parameters, that describe the temperature dependence of viscous and elastic relaxations. The Stickel representation of the viscosity,[46,47] namely $1/\sqrt{\mathrm{d}(\log \eta)/\mathrm{d}(1/T)}$ versus $1000/T$, confirms the occurrence of a single VF behavior. This is illustrated in Figure 4 for R80 and B10.

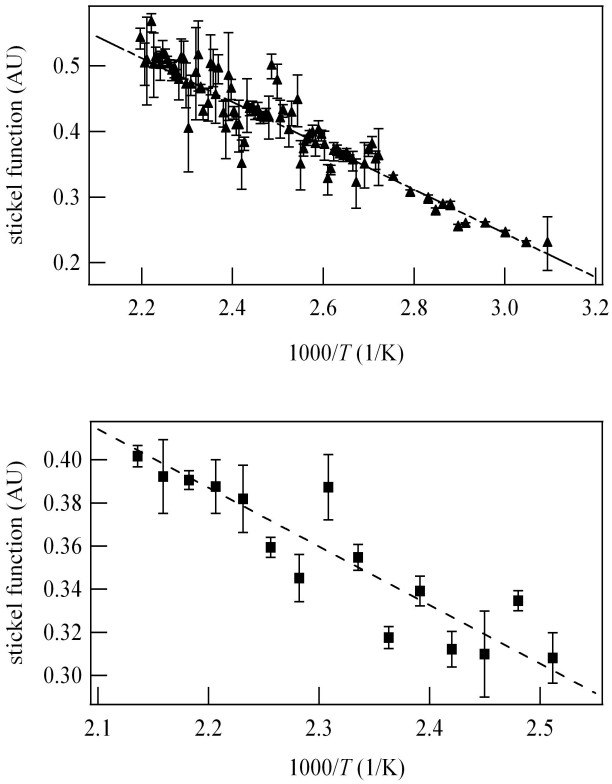

Figure 4. Stickel plot of zero-shear viscosity of R80 (triangles) and B10 (squares).

Figure 3 (bottom) shows the fragility plot[48] of the copolymers together with some literature PMMA homopolymers. In this representation for the viscosity, the fragility index[49] m characterizes the steepness of the slope of $\log\eta$ dependence on T_g/T near T_g: $m=\mathrm{d}(\log\eta(T))/\mathrm{d}(T_g/T)\big|_{T_g}$. A stronger deviation from Arrhenius behavior corresponds to a more fragile system and to a larger m value. It is seen (Figure 3 and Table 3) that the PMMA homopolymers locate in a central region of the plot in which both the random and the block copolymers with lower amounts of MA4 counits are included. On the other hand, a trend is observed in random copolymers exhibiting increasing fragility with the increase in MA4 counit percentage. By contrast, the block copolymers (Table 3) become less fragile (namely stronger) with the increase in MA4 block percentage. This opposite behavior is probably connected with the different configurational entropy of the main chains in the different polymer architectures.[50]

Table 3. VF Parameters of the Investigated Copolymers

sample	variable	η_∞ (Pa s)	T_b (K)	T_0 (K)	m
R90	$\eta(T)$	$(5.10\pm0.60)\times10^{-3}$	1240±40	274±3	162±7
R80	$\eta(T)$	$(8.80\pm0,80)\times10^{-3}$	1480±60	268±3	123±7
R10	$\eta(T)$	$(4.10\pm0.830)\times10^{-4}$	2680±80	272±3	59±4
B20	$\eta(T)$	$(3.00\pm0.050)\times10^{2}$	210±30	330±30	9±4
	$a(T)$	---	1450±50	340±4	---
B10	$\eta(T)$	$(7.24\pm0.050)\times10^{-2}$	1800±250	240±20	13±2
	$a(T)$	---	1950±50	323±3	---
B03	$\eta(T)$	$(1.20\pm0.050)\times10^{-2}$	1880±50	327±3	76±7
PMMA1[a]	$\eta(T)$	---	3530±50	286±1	56±2
PMMA2[b]	$\eta(T)$	---	2920±40	303±1	85±3
PMMA3[c]	$\eta(T)$	---	3220±50	323±1	124±4

[a]About 59% syndiotactic PMMA.[40]
[b]Less than 35% syndiotactic PMMA.[40]
[c]Conventional PMMA.[41]

3.2. ESR Lineshapes.

Figure 5 shows the time evolution of the experimental ESR spectra for R90 and B10. The process was followed until a stable spectrum was eventually reached at the annealing temperatures T_a=358 K for R90 and T_a=387 K for B10. Note that the temperatures T_a were set in the high temperature region of the investigated ranges, in the isotropic state of the liquid crystalline samples. R90 and R80 are characterized by a time evolution of the ESR lineshape during their annealing, as shown in figure 6 for R90. On the other hand, the block copolymers did not exhibit any thermal history dependence (in Figure 5 the B10 case), as well as R10 random copolymer, as a probable consequence of the small perturbation produced on the matrix by the ordering of the mesogenic units in the liquid crystalline phase of the polymer matrices.

From the figure, the sensitivity of the ESR lineshape to local environments is evident. In fact, the lineshapes of the copolymers, excluding R10 that contain a very small amount of

mesogenic MA4 units, signal the presence of two different sites, a slow and a fast one, for the probe reorientation in the polymer matrix (see the vertical dotted lines in Figure 5). The percentage of site population is subjected to time evolution or not, depending on the polymer considered. As an example, a comparison between the stable ESR spectrum of R90 and the initial one shows that the contribution from the slow component of the ESR lineshape increases up to a saturation value as the annealing time increases.

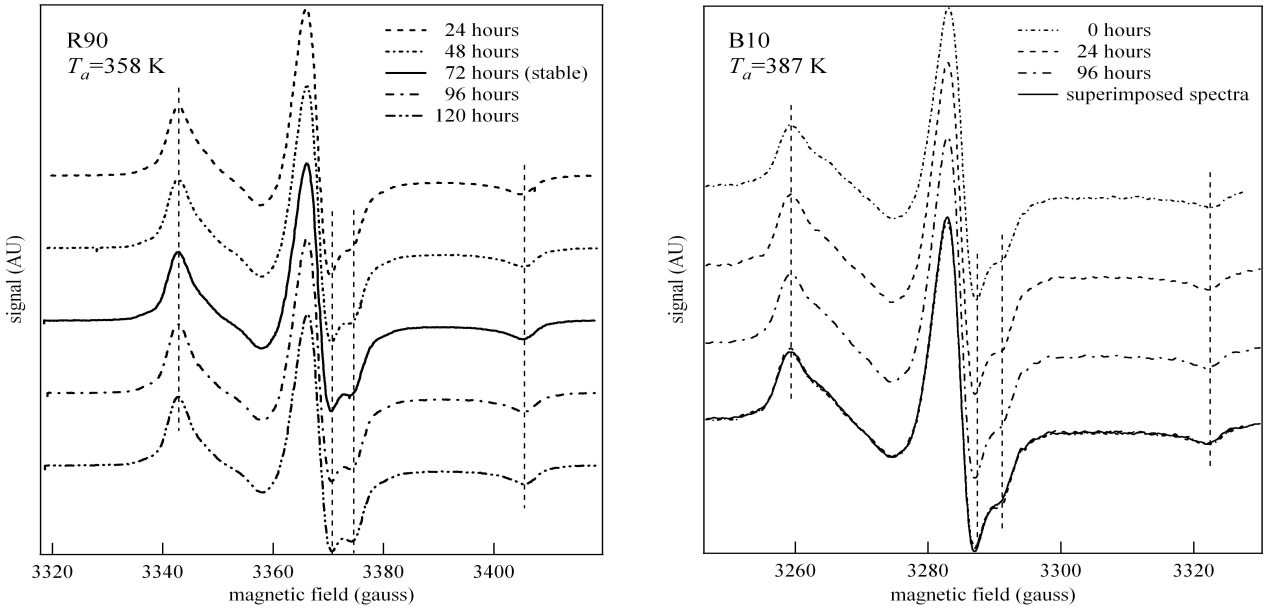

Figure 5. Time evolution of the ESR lineshape. Left: R90 during the annealing at T_a=358 K. Right: B10 during the annealing at T_a=387 K. The stable spectrum is reached by R90 after 72 hours, while B10 does not show any time evolution of the spectra.

For all cases of heterogeneous reorientation, careful simulations were carried out to confirm the bimodal character of the distribution function of the molecular tracer sites.[7,51] In particular, a two δ-like distribution function, with a fast and a slow dynamic components, was shown to provide the best simulation of the ESR spectra.[51]

Table 4. Time Evolution of the Population Percentage of the ESR Spectra of R90 and R80 at T_a

sample	population %	at 0 h	at 24 h	at 48 h	at 72 h (stable)
R90	fast	80%	72%	67%	60%
	slow	20%	28%	33%	40%
R80	fast	63%	61%	58%	55%
	slow	37%	39%	42%	45%

Table 4 summarizes the evolution of the population percentage at T_a=358 K for R90 and R80. One notes that the slow component percentage grows at the expenses of the fast component towards an equilibrium percentage while the values of the spinning correlation times during the annealing time are constant within the experimental error. Therefore, a mechanism of redistribution of the tracers in different molecular sites inside the polymer matrix is responsible for the observed time dependence of the ESR spectra of the polymer matrices with a more distinct liquid crystalline character.

3.3. Rotational Dynamics in Random Copolymers.

The temperature dependence of the spinning correlation time $\tau_{||}$ of the cholestane molecular tracer dissolved in the investigated random copolymers is shown in Figure 6. For the samples characterized by heterogeneous reorientation, the correlation times in the fast and slow molecular sites and the percent population of the fast sites are shown as a function of the temperature.

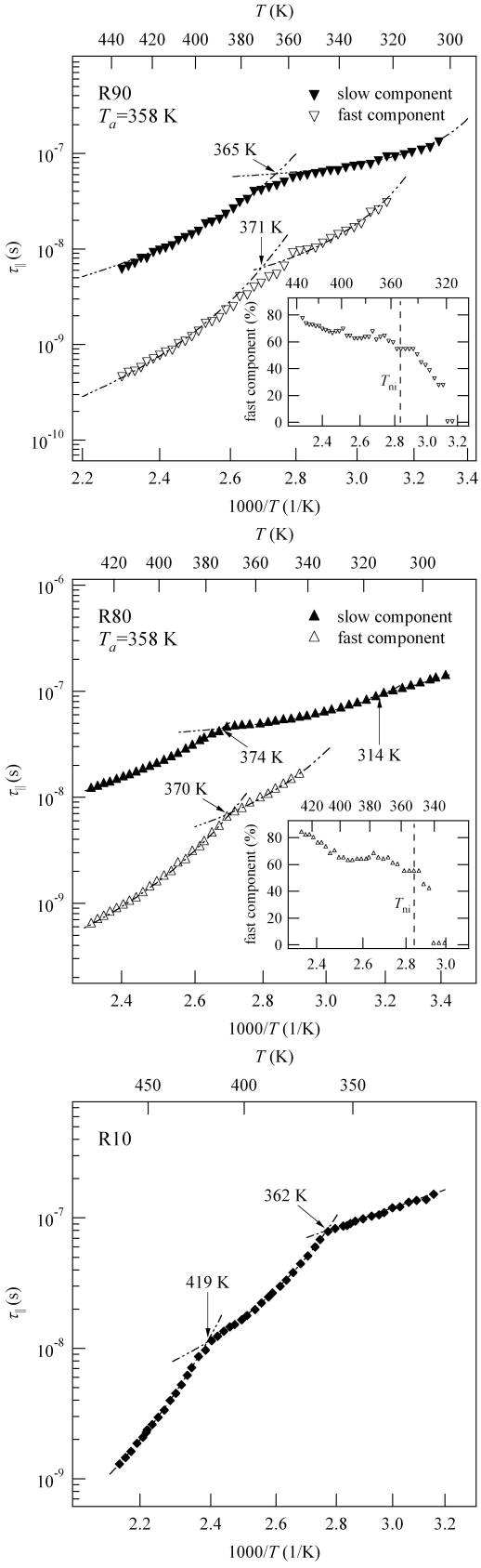

Figure 6. Temperature dependence of ESR correlation times in the R90 (top), R80 (middle), and R10 (bottom) copolymer samples. The insets show the population of the fast dynamic component.

The rotational dynamics in R90 and R80 was investigated from temperatures slightly greater or smaller than T_g. Starting from the highest temperatures, the reorientation appears heterogeneous and suggests a trend towards a collapse to a homogeneous dynamics just at T_g (Figure 6). The reorientation processes in R10 are homogeneous at the nanoscale, as detected by the ESR spectroscopy.

At a general glance at the dynamics trend of the investigated samples, different dynamics regimes are identified for the correlation time behavior, that onset at peculiar temperatures and are reproduced by different laws, as described later in detail. In the presence of heterogeneity, different regimes are also detected for the population percentages.

Firstly, we focus the attention on R90 and R80 that exhibit heterogeneous dynamics. The populations of their fast sites, shown in the insets of Figure 6, show two dynamics regions: (1) a high-temperature region extends between approximately 440 K and the respective T_{ni}, in which the value of the fast component percentage smoothly decreases from about 80% and stabilizes at about 60%–55%; (2) from T_{ni} an intermediate-temperature region develops, where, in correspondence of the quick depletion of the fast sites, the slow sites become more significantly populated on decreasing the temperature. This region covers temperature intervals with very different extension for the two copolymers, namely 10 K for R80 and 35K for R90. The fast population then disappears and, at the lowest temperatures, the rotational dynamics pertains to the slow component only. Thus, the latter appears more persistent than the fast one because it extends over a larger temperature region, that ends at, or includes T_g. We suggest that the relative instability of the fast component in the intermediate-temperature region is due to the increasing strength of the nematic ordering potential in the host matrix as the temperature lowers. The fast reorientation probably occurs at the nematogenic cores, so that the molecular tracer is expelled to the surrounding regions because of its steric hindrance as the available free volume at the mesogenic units decreases on lowering

temperature. The process turns out to be favored as much as the available free volume increases in extension, namely, as much as the mesogenic content in the sample diminishes. This is confirmed by comparing the dynamics over different time scales, as shown below. It is also consistent with previous findings on a PMA4 homopolymer and a R70 copolymer, both subjected to the same thermal annealing at 358 K.[18] In the homopolymer at temperatures above T_{ni}, the fast dynamics stabilized at a population of about 40%–50%, because of the lower volume available for the cholestane at the mesogenic units with respect to R90 and R80. On the other hand, the fast component percentage endured in a larger interval of 20 K below T_{ni}, likewise the present R90. In R70, the fast component stabilized at 30%–40%, a smaller value probably because of the lesser amount of MA4 counits available as sites for the reorientation of the molecular tracer, and it stopped suddenly at T_{ni}, where the nematic phase onsets and the cholestane is expelled away from the mesogenic units. The R80 case results to be an intermediate one between R90 and R70.

In the dependence of the spinning correlation time $\tau_{||}$ of the fast and/or slow components of the molecular tracer on temperature (Figure 6), different dynamics regimes can be identified. The crossover temperatures between the dynamics regions almost coincide with $1.2T_g$. In the following, we will be referring to them as the high- and intermediate-temperature dynamics regions. For the slow component of R80 an additional dynamics regime was observed that develops in the low-temperature region below the crossover temperature T_g, its temperature dependence being reproduced by an Arrhenius[47] behavior: $\tau_{||}=\tau_{||\infty}\exp(\Delta E/RT)$. The activation energy value ΔE evaluated for this region (Table 5) resulted to be in a range characteristic of the cholestane and other spin probes in molecular glasses[34,52] or oligomers[22,53] in a nearly solid-like diffusion rather than in polymer[7] glasses. As one example, at temperatures below T_g, ΔE was usually found to be 31–35 kJ/mol for cholestane reorientation in PMA4 homopolymers and copolymers[15] and various poly(alkyl acrylate)s.[19–21] These values were ascribed to coupling of the spin probe dynamics to secondary relaxation modes of the matrix.[7] It has been proved that cholestane dynamics is more

strongly related to the polymer main backbone relaxation than other molecular tracers of different shape and size.[22] Therefore the present values of ΔE suggest a sort of segregation mechanism in this temperature region and/or a very local dynamics where the relevant features are driven by small numbers of units in a cage with dynamic characteristics similar to those of molecular glass formers.

In Table 5, it is seen that the crossover temperatures signaling dynamic anomalies between the intermediate- and high-temperature regions are located at about $1.2T_g$, with values for the slow component rotational correlation time (about 10^{-7} s) virtually coincident with the universal "magic" relaxation time $\tau(T_c)$, that marks the dynamic crossover from liquid-like to solid-like behavior of glass formers.[54] T_c is the critical temperature of the mode coupling theory.[55] We have found a very similar behavior, with the same cholestane probe, in several other polymers such as PPG,[22] PMA,[20] PnBA,[19] PEA,[18] and some liquid crystalline polymethacrylates,[7,11,15] where the crossover was ascribed to the onset of cooperativity. It should be emphasized that in all the quoted cases the crossover temperatures were found to be near the value $1.2T_g$, where the critical temperature of mode coupling theory T_c is usually found and where dynamic heterogeneities become appreciable on the nanometer length scale also in polymer samples with homogeneous architecture and glasses.[56]

In both high- and intermediate-temperature regions, the temperature behavior of $\tau_{\|}$ for the cholestane sites could be reproduced fairly well by assuming a VF law[44] (see eq 1):

$$\tau_{\|}(T) = \tau_{\|\infty} \exp\left(\frac{T_b}{T - T_0}\right) \qquad (2)$$

The values of the fit parameters are reported in Table 5 for both slow and fast dynamic components of R90 and R80 samples, along with the ranges of temperature of the dynamics regions. T_0 resulted in all cases coincident with the corresponding Vogel temperature obtained by means of rheology measurements, signaling in such a way that the rotational relaxation is driven by the dynamics of the polymer main chain. As a consequence, in both high- and intermediate-temperature regions, and for the fast and slow dynamic components, the spinning correlation time behavior can be expressed

as a fractional law of the viscosity:

$$\tau_{\parallel}(T) \propto [\eta(T)]^{\xi} \quad (3)$$

where ξ, the fractional exponent, may vary between 0 and 1, with ξ=1 corresponding to a complete coupling of the molecular tracer dynamics to the terminal viscosity relaxation of the host matrix. ξ resorts to be the ratio of the T_b of the VF law relevant to the dynamics of the rotational dynamic component over the value of the pseudo-activation temperature pertinent to the sample viscosity. In this way, the values of the fractional exponent ξ were calculated for the random copolymers and are given in Table 5.

Table 5. Dynamics Details and Parameters of the Random Copolymers

sample	region[a]	law[b]	T range (K)	$\tau_{\parallel\infty}$x10^{10} (s)	T_0 (K)	T_b (K)	ξ	ΔE (kJ mol^{-1})
R90	HT(F)	VF	434–371	(6.7±0.2)x10^{-12}	270±8	693±50	0.45±0.04	---
	IT(F)	VF	371–322	(2.4±0.2)x10^{-9}	270±8	180±16	0.10±0.01	---
	HT(S)	VF	434–365	(3.6±0.2)x10^{-10}	270±8	486±20	0.39±0.02	---
	IT(S)	VF	365–304	(3.9±0.2)x10^{-8}	270±8	42±5	0.04±0.01	---
R80	HT(F)	VF	430–370	(1.0±0.2)x10^{-11}	265±9	690±60	0.45±0.04	---
	IT(F)	VF	370–343	(5.9±0.2)x10^{-10}	265±7	235±20	0.18±0.02	---
	HT(S)	VF	430–374	(9.8±0.2)x10^{-10}	265±7	415±20	0.26±0.02	---
	IT(S)	VF	374–314	(2.4±0.2)x10^{-8}	265±8	67±7	0.04±0.01	---
	LT(S)	Arr	314–293	(3.3±0.2)x10^{-10}	---	---	---	15.0±0.5
R10	HT	VF	466–419	(1.7±0.1)x10^{-12}	272±6	1270±50	0.48±0.03	---
	IT	VF	419–362	(5.1±0.2)x10^{-10}	272±6	450±20	0.17±0.01	---
	LT	Arr	362–316	(7.4±0.2)x10^{-10}	---	---	---	14.0±0.5

[a]Key: high-temperature (HT); intermediate-temperature (IT); low-temperature (LT) region. Slow (S) or fast (F) component is also specified.
[b]Arrhenius or VF (eq 2) behavior.

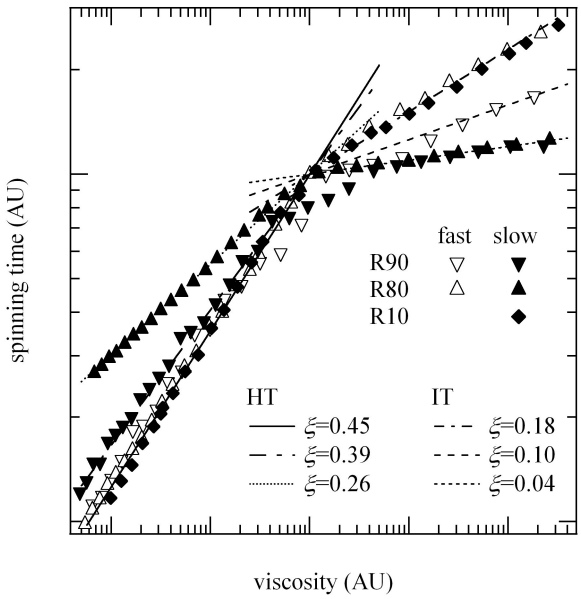

Figure 7. Crossover region for cholestane in random copolymers: spinning correlation times versus viscosity. Power law fits are superimposed.

The crossover regions are better shown in Figure 7, where the fast and slow rotational correlation times are directly plotted versus η. Many reports on fractional diffusion laws in many different glass-forming systems have appeared in the literature using ESR spectroscopy[16–22,24,34,57] and other[58] experimental techniques. Furthermore, recent theoretical and numerical studies on different glass former models evidenced the presence of decoupling phenomena in transport properties,[59] invoking a crucial role of the growing length scale typical of the heterogeneous and cooperative character of dynamics. To our knowledge, the occurrence of complete coupling between the tracer reorientational dynamics and structural relaxation processes or viscosity in the polymer matrix, over a large range of high temperatures, has been demonstrated in a very few cases[22,23] and was only inferred[53] in a PMA4 oligomer. Regarding liquid crystalline polymers, it was shown that, in the highest temperature regions, the decoupling of the dynamics of the molecular tracer dissolved in the PMA4 homopolymer should be ascribed to a steric hindrance due to the specific local characteristic of the host matrix, rather than to a cooperativity effect in dynamics.[7] The cooperative effects onset in the intermediate-temperature (mostly nematic) region. Here the

dynamics is still driven by the polymer main chain, as deduced by the common value of the Vogel temperature, but the fractional exponent ξ lowers, accounting for both the steric and the cooperative effects due to the ordering of the polymer side groups driven by the nematic potential.[7] The same interpretation can be adopted in the present study. More specifically, in the high-temperature (isotropic) region and for the fast component of the molecular reorientation, the decoupling degree between cholestane dynamics and PMA4 random copolymer viscosities turned out to be $\xi_{HT(F)}$=0.45 for both R90 and R80 (Table 5). The value is consistent with the R70 case ($\xi_{HT(F)}$=0.52),[60] and shows a possible similarity with the homopolymer case ($\xi_{HT(F)}$=0.61) after the thermal treatment at 358 K.[61] The relatively high value of $\xi_{HT(F)}$, together with the clear sensitivity of the probe dynamics to the nematic-to-isotropic transition, located near $1.2T_g$, strengthens the hypothesis that the sites experienced by the molecular tracer in these liquid crystalline polymers may be located among the mesogenic side groups. This appears also in agreement with previous observations on a closely related nematic polyacrylate.[62] Most importantly, the result validates the interpretation given in discussing the populations of the fast sites. In Table 5, the fractional exponents $\xi_{IT(F)}$ are also reported for the fast sites of R90 and R80 in the intermediate-temperature region. It is seen that the copolymers have slightly different values of the power law exponents.

Regarding the slow component of the molecular reorientation in the high-temperature region, the smaller value evaluated for T_b (Table 5) implies a greater decoupling from the structural relaxation dynamics, despite the slower dynamics of the probe. Accordingly, the slow sites are likely situated away from the mesogenic unit. In this case, the onset of the nematic potential is experienced by the molecular tracer in the dynamic sites in a smooth way so that, according to the results on population, no expulsion is induced because of the steric interplay between cholestane and polymer matrix. For the slow component in the high-temperature region, the decoupling degree between cholestane dynamics and PMA4 random copolymer viscosities turned out to be $\xi_{HT(S)}$=0.39 and $\xi_{HT(S)}$=0.26 for R90 and R80 respectively (Table 5). This decreasing trend collocates these

values between the highest ones, exhibited by homopolymers[61] ($\xi_{HT(S)}$=0.41), and the smallest ones, found in random copolymers with smaller percentage of MA4 counits: $\xi_{HT(S)}$=0.18 in R70 and $\xi_{HT(S)}$=0.13 in R60.[60,63] This could be due to the softening of the "cages", which collectively host the slow reorientational sites, when the number of mesogenic units in the copolymer is lowered. The slow component of the cholestane dynamics in the intermediate-temperature region, because of the poor coupling to the main polymer relaxation, results in low fractionary exponents $\xi_{IT(S)}$ (Table 5) in agreement with the ones found in other random PMA4 copolymers.[63]

A different scenario is available with the dynamics of R10 (Figure 6), where the mesogenic unit percentage is low and the polymer matrix does not evidence any liquid crystalline feature, both at a macroscopic length scale, as detected by DSC and rheological measurements, and at nanoscale, as detected by ESR spectroscopy. The rotational dynamics of the molecular tracer appears homogeneous as for molecular glass formers, low molecular weight polymer glass formers[16,17,22,24,34,57,63,64] and non mesogenic polymer[18−21,23] matrices. Three dynamics regions are identified: a high temperature VF region down to the crossover at $1.22T_g$, another VF region at intermediate temperatures ranging from $1.22T_g$ to $1.10T_g$, and finally an Arrhenius regime, below T_g. This last shows a ΔE of 14 kJ/mol, comparable to the R80 case. The $\tau_{||}$ values cover a dynamics range that approximately includes the variations of both fast and slow component dynamics in R90 and R80, taken together.

One notes the temperatures at which the dynamics anomalies occur. The first one from above locates at $1.22T_g$, once again, where mode coupling theory would locate its critical temperare.[55] Therefore, we have confirmation that the decoupling phenomenon at high temperatures in random copolymers is independent of the liquid-crystalline character of the material. It may rather be ascribed to cooperative phenomena occurring in amorphous materials as the temperature is lowered.[65] The second crossover, from VF to the Arrhenius regime, falls at a value very near the T_g temperature of PMMA. This last finding, and the small amount of PMA4 counits, suggest that R10

dynamic behavior should be mainly related to dynamic processes present in a neat PMMA polymer, rather than in PMA4 homopolymers. This is also well supported by the value of the Vogel temperature T_0, from both ESR and rheology measurements, that is close to these of PMMAs, and by the T_bs of the high- and intermediate-temperature regions, that provide ξ values in agreement with the ones pertinent to poly(alkyl acrylate) matrices.[21]

3.4. Cooperativity Index and Packing Length.

Cooperativity effects in the nematic region are accounted for by defining a cooperativity coefficient ξ_C,[7] equal to ξ_{IT}/ξ_{HT}, where ξ_{HT} and ξ_{IT} are the fractionary coefficients in eq 3 relevant to the high- and intermediate-temperature regions, respectively. In turn, a cooperativity index $\kappa=1/\xi_C$, is defined to provide an estimation of the cooperative units involved in this structural relaxation.[7] In Table 6, the values of κ are reported for a series of random copolymers and PMA4 homopolymer,[6,15,66] and a series of poly(alkyl acrylate)s as well.[21] The random copolymers series include homogeneous and heterogeneous systems, depending on the percentage of mesogenic counit MA4.

The attention is devoted to the homogeneous non mesogenic polymers and to the slow sites of the heterogeneous polymers, because these sites for the reorientation of the molecular tracer pertain to non ordered regions of the materials. It is seen from Table 6, that the collection of data can be roughly separated in two sets. A first set includes highly cooperative polymers, with a number of rearranging units involved in the structural relaxation of the polymer matrix $\kappa\geq6$: R90 and R80, with high content of mesogenic counits, and PMA4 homopolymer. On the other hand, a second set with values of the cooperativity index $\kappa\leq3$ identifies polymers that exhibit poor or not-existent liquid crystalline properties and a similar architecture, such as for the poly(alkyl acrylate) series.

The effect of the PMA4 microstructure over the relaxation properties of the material was

recently shown considering the polymer chain entanglement in the framework of the packing length p.[67] Values of the packing length of the polymers are reported in Table 6.[26,67,68] It appears that the packing length correlates with the number of cooperative units κ and that a threshold separates the two sets of polymers. Note that the value of packing length p=1.0 nm corresponds to a semiaxis dimension of the molecular tracer cholestane.

Table 6. Cooperativity Coefficients ξ_C, Cooperativity Indices $\kappa=1/\xi_C$, and Packing Lengths p for PMA4 Homopolymer, Random PMA4 Copolymers, and Poly(Alkyl Acrylate)s

sample	homogeneity	ξ_C [b]	$\kappa=1/\xi_C$	p (nm)
PMA4 homopolymer[a]	no	0.18	6	>0.93
R90[a]	no	0.10	10	1.22
R80[a]	no	0.15	7	1.14
R70[a]	no	0.32	3	1.01
R60	no	0.52	2	0.87
R10	yes	0.35	3	0.45
PMA	yes	0.39	3	0.34
PEA	yes	0.41	2	0.37
PnBA	yes	0.39	3	0.47

[a]Annealed at T_a=358 K.
[b]ξ_C calculated for the slow component in case of non homogeneous samples.

3.5. Rotational Dynamics in Block Copolymers.

The spinning correlation times of cholestane in block copolymers, investigated in a range of temperatures that extends to above T_{ni}, are shown in Figure 8. As a first consideration, the dynamics looks heterogeneous, with a fast site and a slow one for the reorientation of the molecular tracer, at all the investigated compositions of PMA4 and PMMA blocks. This means that in the block copolymers the probe experiences the presence of nematic domains formed by the MA4 blocks, independent of their concentration. In comparison with the ESR dynamics observed in random copolymers, it can be noted that the rotational relaxation is not homogeneous in B10, while it is

homogeneous in R10 and in random copolymers rich up to 60 mol% of MA4.[11] Thus, ESR spectroscopy is very sensitive to local environment in which the molecular tracer is embedded and is able to provide distinct responses in samples with the same molar composition but with different architectures. As a matter of fact, the microphase separation in block copolymers and the subsequent confinement in submicron/nanoscale domains favor the segregation of molecular tracers in the discrete minority phase formed by the nematogenic MA4 blocks, even at low concentrations.

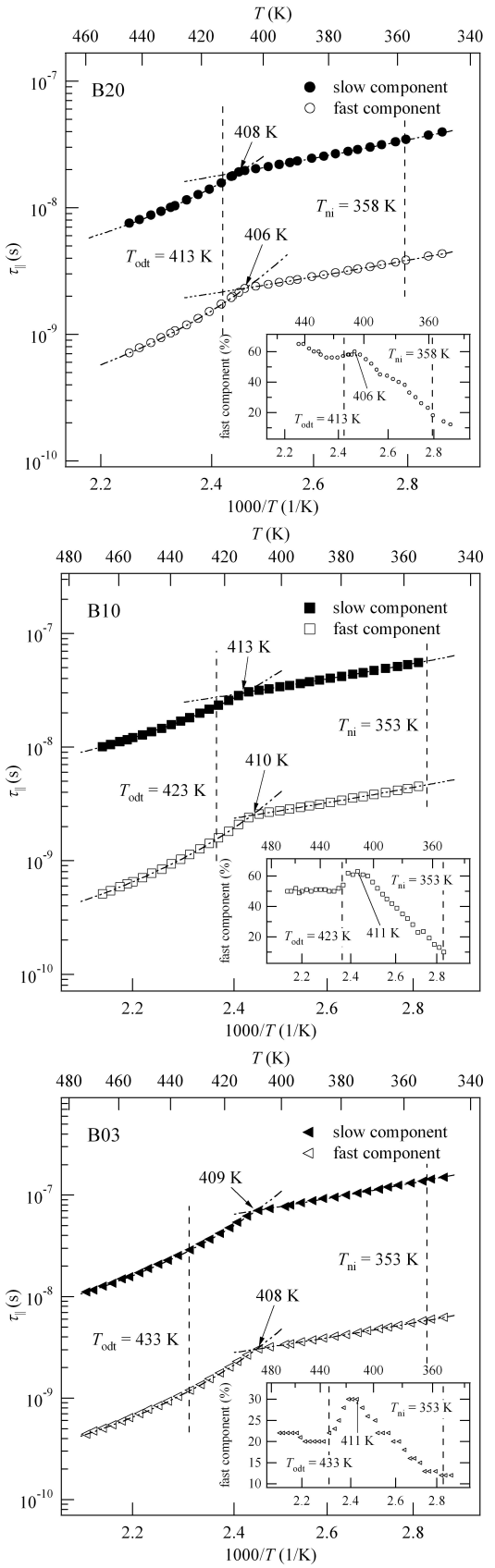

Figure 8. Temperature dependence of ESR correlation times in B20 (top), B10 (middle), and B03 (bottom) copolymers. The insets show the population of the fast component.

As a second consideration, the very similar behavior, both in shape and in magnitude, of the correlation times with temperature in block copolymers can be appreciated. For all the investigated samples and for temperatures higher than T_g^{PMA4} (Table 1), the dynamics of the cholestane was completely characterized in fast and slow sites, imputable to the molecular rotation in the different separated microphases, and the relative populations were evaluated. For both dynamic components, two regions were identified for the temperature dependence of the correlation times. In analogy with the random copolymers, where Arrhenius trends are observed at the lowest temperatures, the two dynamics temperature regions are referred to as the intermediate- (IT) and the low-temperature (LT) regions. The dynamics anomaly that separates IT and LT regions is located between T_g^{PMMA} and the order-to-disorder transition temperature T_{odt} for PMA4 block copolymers (Table 1). More precisely, the crossover sets in at about $1.2T_g^{PMA4}$. Actually, in the random copolymers this same temperature separates two VF regimes. Therefore, a series of different competing interactions can play a role in the crossover temperature range, such as either the cooperative processes related to the liquid crystal phase of the minority PMA4 phase or local relaxations driven by the glassy state of PMMA.

Below the crossover temperature, the dynamics follows an activated Arrhenius regime. Its onset is usually ascribed to the coupling of the tracer dynamics to closely localized relaxation processes[69] that, in the present case, affect and drive equally both dynamic sites. The activation energies ΔE are about 14 kJ mol^{-1} (Table 7), much lower than the ΔE values in the range 33−38 kJ mol^{-1} found in random copolymers[7,15] and in linear poly(alkyl acrylate) homopolymers for activated Arrhenius regimes.[20,21] They also do not agree with values reported for PMMA polymers.[69] On increasing temperature, the ordered microstructure softens and vanishes, so that, at temperatures higher than $T_{odt}>T_g^{PMMA}$, the dynamics becomes somewhat sensitive to a collective relaxation of the polymer matrix, as signaled by the VF temperature dependence of the cholestane reorientation.

These findings are in agreement with the ability of the ESR probe spectroscopy to track the host relaxation process with the nearest time scale to the molecular reorientation.[23] The VF dynamics regions, Vogel temperatures T_0 and activation pseudo-activation temperatures T_b are reported in Table 7.

Table 7. Dynamic Details and Parameters of the Block Copolymers

sample	region[a]	law[b]	T range (K)	$\tau_{\parallel\infty}$x10^{10} (s)	T_0 (K)	T_b (K)	ξ	ΔE (kJ mol^{-1})
B20	IT(F)	VF	445–406	(2.5±0.2)x10^{-11}	340±7	200±20	0.14±0.01	---
	LT(F)	Arr	406–347	(5.5±0.2)x10^{-11}	---	---	---	14±1
	IT(S)	VF	445–408	(4.7±0.2)x10^{-10}	340±7	180±25	0.12±0.02	---
	LT(S)	Arr	408–347	(3.1±0.2)x10^{-10}	---	---	---	15±1
B10	IT(F)	VF	467–410	(2.2±0.2)x10^{-11}	323±7	350±30	0.18±0.02	---
	LT(F)	Arr	410–357	(5.5±0.2)x10^{-11}	---	---	---	13±1
	IT(S)	VF	467–413	(9.8±0.2)x10^{-10}	323±7	260±25	0.13±0.01	---
	LT(S)	Arr	413–357	(2.4±0.2)x10^{-8}	---	---	---	13±1
B03	IT(F)	VF	476–408	(3.7±0.2)x10^{-11}	325±7	370±20	0.20±0.01	---
	LT(F)	Arr	408–347	(4.9±0.2)x10^{-11}	---	---	---	14±1
	IT(S)	VF	476–409	(1.0±0.1)x10^{-9}	325±7	355±20	0.19±0.01	---
	LT(S)	Arr	409–347	(9.2±0.2)x10^{-10}	---	---	---	15±1

[a]Key: intermediate-temperature (IT); low-temperature (LT) region. Slow (S) or fast (F) component is also specified.
[b]Arrhenius or VF (eq 2) behavior.

Following the study on random copolymers (Table 3), an attempt to evaluate the degree of coupling to the structural relaxation of the matrix for the sites of the block copolymers was carried out by considering a rescaling with respect to the viscosity of the corresponding matrix. For the B03 copolymer, with the smallest amount of MA4 counit, this procedure is a smooth one, in that the TTS principle holds and the T_0 values for VF laws from viscosity and ESR spectroscopy coincide. It is found that the ξ values for fast and slow sites in the IT range compare with $\xi_{IT(F)}$ of the fast component of R90 and R80, suggesting location of the fast sites of B03 in the same matrix

environment as the ones of R90 and R80, namely at the mesogenic domains of the polymer matrix.

The cases of B10 and B20 are more complicated because of their thermorheological[47] complexity. Although the viscosity curves vs temperature were obtained by creep and flow experiments without recurring to shifting procedures, in B10 T_0s are different in the VF laws obtained for the viscosity and the ESR molecular reorientation. This provides a clear indication that non local relaxations, such as the ones pertinent to the long-time dynamics of the chain, are not adequate observables for the study of scaling laws in block copolymers. In other words, the molecular tracer dynamics is driven by more local motions of the host matrix. However, the $a(T)$ function (Table 3) of G' master curves and the rotational correlation times have coincident T_0 values. Accordingly, the rescaling procedure provided ξ_{IT} values comparable to those of the B03 case. In the light of the results with B10, B20 is handled considering the VF parameters from $a(T)$. The ξ_{IT} values for fast and slow sites result comparable to the values of the other block copolymers that are slightly diminishing as the percentage of MA4 counits increases.

The temperature dependence of the fast site population deserves some consideration (insets of Figure 8). Starting from the high temperatures, well above both T_{odt} and T_{ni}, the mean percentages of fast sites seem leveled off at plateau values that depend on the percentage of MA4 counits. In particular, the higher the content of mesogenic counits, the higher the percentage of fast sites in the sample. Starting from T_{odt} an increase in fast sites is detected, most pronounced in B10 and B03 samples that possess the greater percentages of MMA counits. This suggests that the ordering process that takes place in the non mesogenic constituent of the block copolymer makes available more free volume in the mesogenic part where more molecular tracers are placed. As a consequence, the fast sites are located in the mesogenic block of the copolymer. On decreasing the temperature, a maximum is reached, then the percentages of the fast component decrease smoothly, signaling that in this temperature region a mesogenic ordering plays a role analogous to the one observed for random copolymers. In fact, by inspection of Figure 7, it is possible to recognize that

the fast sites of all block copolymers disappear at temperatures close to 358 K, that is at the T_{ni} in the nematic block copolymers (Table 1).

5. CONCLUDING REMARKS

The resolution of the ESR spectroscopy allowed a thorough characterization of the cholestane spin probe reorientation in fast and slow molecular sites with different relative populations over large temperature ranges. Moreover, the different architectures and molecular structures of copolymers manifest themselves in the heterogeneity persistent even at low concentration of MA4 counit in block copolymers, as an unequivocal signature of microphase separation and confinement in submicron/nanoscale domains. The emerging picture is that of greatly heterogeneous copolymer systems as far as site and cooperativity are concerned. While in random copolymers the heterogeneity is modulated by the presence of a sufficient amount of MA4 counits, in block copolymers the leading structural property is the ability of self-assembling in supramolecular structures.

The evaluated decoupling degrees of the correlation times from the structural relaxation dynamics or from viscosity suggested the mechanisms relevant to the relaxation. In block copolymers, where the chain dynamics is complicated by the different monomeric friction coefficients of the two blocks, the rotational dynamics is driven by and coupled to more local relaxation processes of the polymer matrix. In random copolymers, the cooperativity is related to the geometric and topologic properties of the polymer chain in the framework of the tube theories of the polymer melts. Finally, the analysis of the dynamics signatures and the coupling data provided in all cases a convenient characterization and a location of the sites available for the molecular reorientation.

In conclusion, the ESR investigation of the rotational motion of the cholestane dissolved in

MA4-MMA random and block copolymers is a suitable tool to identify dynamics and heterogeneity of the host matrices in view of their fundamental and applied interest. The richness of information obtained on these materials in this study is now available for the comprehension of their nanometer/nanosecond scale behavior on a fundamental ground, and for the provision of guidelines to their correct application as substrates for optical nanorecording.

ACKNOWLEDGEMENT

Work partially supported by the Italian MIUR (PRIN 2010–2011).

Notes and References

(1) Eich, M.; Wendorff, J. H.; Reck, B.; Ringsdorf, H. *Makromol. Chem., Rapid Commun.* **1987**, *8*, 59–63.

(2) For recent reviews, see: Shibaev, V. P. *Polym. Sci. Ser. A* **2014**, *56*, 727; Yu, H. *Progr. Polym. Sci.* **2014**, *39*, 781–815.

(3) For one latest example, see Yu, Z.; Hecht, S. *J. Polym. Sci., Part A: Polym. Chem.* **2015**, *53*, 313–318.

(4) Menghetti, S.; Alderighi, M.; Galli, G.; Tantussi, F.; Morandini, M.; Fuso, F.; Allegrini, M. *J. Mater. Chem.* **2012**, *22*, 14510–14517.

(5) Tantussi, F.; Menghetti, S.; Caldi, E.; Fuso, F.; Allegrini, M.; Galli, G. *Appl. Phys. Lett.* **2012**, *100*, 083103.

(6) Andreozzi, L.; Faetti, M.; Galli, G.; Giordano, M.; Palazzuoli, D. *Macromol. Symp.* **2004**, *218*, 323–332.

(7) Andreozzi, L.; Faetti, M.; Galli, G.; Giordano, M.; Palazzuoli, D. *Macromolecules* **2001**, *34*, 7325–7330.

(8) Andreozzi, L.; Faetti, M.; Giordano, M.; Palazzuoli, D.; Zulli, F. *Macromolecules* **2003**, *36*, 7379–7387.

(9) Andreozzi, L.; Autiero, C.; Faetti, M.; Galli, G.; Giordano, M.; Zulli, F. *Macromol. Symp.* **2008**, *263*, 78–85.

(10) Andreozzi, L.; Autiero, C.; Faetti, M.; Galli, G.; Giordano, M.; Zulli, F. *Mol. Cryst. Liquid Cryst.* **2009**, *500*, 63–72. Andreozzi, L.; Faetti, M.; Giordano, M.; Zulli, F. *Eur. Phys. J. B* **2004**, *41*, 383–393. Andreozzi, L.; Faetti, M.; Giordano, M.; Palazzuoli, D.; Laus, M.; Galli, G. *Mol. Cryst. Liquid Cryst.* **2003**, *398*, 97–106.

(11) Andreozzi, L.; Autiero, C.; Faetti, M.; Giordano, M.; Zulli, F; Galli, G. *Mol. Cryst. Liquid Cryst.* **2006**, *450*, 363–371.

(12) Berliner, L. J. *Spin Labeling: Theory and Application I*; Academic Press: New York, 1976. Berliner, L. J. *Spin Labeling: Theory and Application II*; Academic Press: New York, 1979.

(13) Moro, G.; Freed, J. H. *J. Phys. Chem.* **1980**, *84*, 2837–2840. Moro, G.; Freed, J. H. *J. Chem. Phys.* **1981**, 7*4*, 3757–3773. Lee, M. H.; Kim, I. M.; Dekeyser, R. *Phys. Rev. Lett.* **1984**, *52*, 1579. Lee, M. H.; Kim, I. M.; Dekeyser, R. *Phys. Rev. Lett.* **1984**, *52*, 2191.

(14) Andreozzi, L.; Camorani, P.; Faetti, M.; Palazzuoli, D. *Mol. Cryst. Liquid Cryst.* **2002**, *375*, 129–142.

(15) Andreozzi, L.; Faetti, M.; Giordano, M.; Palazzuoli, D.; Zulli, F; Galli, G. *Mol. Cryst. Liquid Cryst.* **2005**, *429*, 21–29.

(16) Andreozzi, L.; Di Schino, A.; Giordano, M.; Leporini, D. *Europhys. Lett.* **1997**, *38*, 669–674.

(17) Andreozzi, L.; Bagnoli, M.; Faetti, M.; Giordano, M. *J. Non-Cryst. Solids* **2002**, *303*, 262–269.

(18) Andreozzi, L.; Castelvetro, V.; Faetti, M.; Giordano, M.; Zulli, F. *Philos. Mag.* **2004**, *84*, 1555–1565.

(19) Andreozzi, L.; Autiero, C.; Faetti, M.; Giordano, M.; Zulli, F. *J. Phys.: Condens. Matter* **2006**, *18*, 6481–6492.

(20) Andreozzi, L.; Autiero, C.; Faetti, M.; Giordano, M.; Zulli F. *J. Non-Cryst. Solids* **2006**, *352*, 5050–5054.

(21) Andreozzi, L.; Autiero, C.; Faetti, M.; Giordano, M.; Zulli, F. *Philos. Mag.* **2007**, *87*, 799–810.

(22) Andreozzi, L.; Faetti, M.; Giordano, M.; Zulli, F. *J. Phys. Chem. B* **2010**, *114*, 12833–12839.

(23) Faetti, M.; Giordano, M.; Leporini, D.; Pardi, L. *Macromolecules* **1999**, *32*, 1876–1882.

(24) Bartos, J.; Andreozzi, L.; Faetti, M.; Sausa, O.; Racko, D.; Kristiak, J. *J. Non-Cryst. Solids* **2006**, *352*, 4785–4789.

(25) Angeloni, A. S.; Caretti, D.; Laus, M.; Chiellini, E.; Galli, G. *J. Polym. Sci., Part A: Polym. Chem.* **1991**, *29*, 1865–1873.

(26) Andreozzi, L.; Galli, G.; Giordano, M.; Zulli, F. *Macromolecules* **2013**, *46*, 5003−5017.

(27) Wunderlich, B. In *Assignment of the Glass Transition*; Seyler, R. J., Ed.; Ed. Am. Soc. Testing and Materials: 1994.

(28) Richardson, M. J.; Savill, N. G. *Polymer* **1975**, *16*, 753–757.

(29) Höhne, G.; Hemminger, V. F.; Flammersheim, H.-J. *Differential Scanning Calorimetry*; Springer-Verlag: Berlin, 2003.

(30) Morrison, F. A. *Understanding Rheology*; Oxford University Press: Oxford, 2001.

(31) Zulli, F.; Andreozzi, L.; Passaglia, E.; Augier, S.; Giordano, M. *J. Appl. Polym. Sci.* **2013**, *127*, 1423–1432. Augier, S.; Coiai, S.; Passaglia, E.; Ciardelli, F.; Zulli, F.; Andreozzi, L.; Giordano, M. *Polymer International* **2010**, *59*, 1499–1505.

(32) Andreozzi, L.; Autiero, C.; Faetti, M.; Galli, G.; Giordano, M.; Menghetti, S.; Zulli, F. *Mol. Cryst. Liq. Cryst.* **2011**, *549*, 133–139.

(33) Andreozzi, L.; Faetti, M.; Giordano, M.; Zulli, F. *Macromolecules* **2004**, *37*, 8010–8016

(34) Andreozzi, L.; Faetti, M.; Giordano, M.; Leporini, D. *J. Phys. Chem. B* **1999**, *103*, 4097–4103.

(35) Andreozzi, L.; Giordano, M.; Leporini, D. *Appl. Magn. Reson.* **1992**, *4*, 279–295.

(36) Andreozzi, L.; Giordano, M.; Leporini, D. In *Structure and Transport Properties in Organized Materials*; Chiellini, E., Giordano, M., Leporini, D., Eds.; World Scientific: Singapore, 1997; p 207.

(37) Perrin, J. *J. Phys. Radium* **1934**, *5*, 497–511. Favro, L. D. *Phys. Rev.* **1960**, *119*, 53–62.

(38) Polnaszek, C. F.; Marsh, D.; Smith, I. C. P. *J. Magn. Reson.* **1981**, *43*, 54–64. Robinson, G. H.;

Dalton, L. R. *Chem. Phys.* **1981**, *54*, 253–259.

(39) Siderer, Y.; Luz, Z. *J. Magn. Res.* **1980**, *37*, 449–463.

(40) Fuchs, K.; Friedrich, C.; Weese, J. *Macromolecules* **1996**, *29*, 5893−5910.

(41) Wu, S. *J. Polym. Sci., Polym. Phys. Ed.* **1989**, *27*, 723–741.

(42) Hiemenz, P. C.; Lodge, T. P. *Polymer Chemistry*, 2nd ed.; Taylor& Francis: Boca Raton, FL, 2007; p 486−491.

(43) Grounds for occurrence of TTS or its failure in polymers and liquid crystalline copolymers has been extensively discussed in Ref. 26, Ref. 9, and references therein.

(44) Vogel, H. *Z. Phys.* **1921**, *22*, 645–646. Fulcher, G.S. *J. Am. Ceram. Soc.* **1925**, *8*, 339–345. Tamman, G.; Hesse, W. *Z. Anorg. Allg. Chem.* **1926**, 156, 245–257.

(45) Honerkamp, J.; Weese, J. *Rheol. Acta* **1993**, *32*, 57–64.

(46) Stickel, F.; Fischer, E. W.; Richert, R. *J. Chem. Phys.* **1995**, *102*, 6251–6257.

(47) Ngai, K. L. *Relaxation and Diffusion in Complex Systems*; Springer: New York, 2011.

(48) Angell, C. A. *J. Non-Cryst. Solids* **1985**, *73*, 1–17.

(49) Angell, C. A. In *Relaxation in Complex Systems*; Ngai, K. L., Wright, G. B., Eds.; Springer: National Technical Information Service, 1985; p 3.

(50) Moynian, C. T.; Angell, C. A. *J. Non-Cryst. Solids* **2000**, *274*, 131–138. Kunal, K.; Robertson, C. G.; Pawlus, S.; Hahn, S. F.; Sokolov, A. P. *Macromolecules* **2008**, *41*, 7232–7238.

(51) Andreozzi, L.; Giordano, M.; Faetti, M.; Palazzuoli, D. *Appl. Magn. Reson.* **2002**, *22*, 71–87.

(52) Andreozzi, L.; Faetti, M., Giordano, M. *Recent Res. Devel. Physical Chem.* **2001**, *5*, 219–254. Andreozzi, L.; Bagnoli, M.; Faetti, M.; Giordano, M. *Philos. Mag. B* **2002**, *82*, 409–419. Andreozzi, L.; Di Schino, A.; Giordano, M.; Leporini, D. *J. Phys.: Condens. Matter* **1996**, *8*, 9605–9608.

(53) Andreozzi, L.; Autiero, C.; Faetti, M.; Giordano, M.; Zulli, F.; Szanka, I.; Galli, G. *Mol. Cryst. Liq. Cryst.* **2007**, *465*, 25–35.

(54) Novikov, V. N.; Sokolov, A. P. *Phys. Rev. E* **2003**, *67*, 031507.

(55) Götze, W.; Sjögren, L. *Rep. Prog. Phys.* **1992**, *55*, 241–376.

(56) As examples, see: Sillescu, H.; Böhmer, R.; Diezemann, G.; Hinze, G. *J. Non-Cryst. Solids* **2002**, *307*, 16–23; Schröter, K. *J. Non-Cryst. Solids* **2006**, *352*, 3249–3254; Donati, C.; Glotzer, S. C.; Poole, P. H.; Kob, W.; Plimpton, S. *J. Phys. Rev. E* **1999**, *60*, 3107–3119; Doliwa, B.; Heuer, A. *Phys. Rev. E* **2000**, *61*, 6898–6908; Berthier, L.; Biroli, G.; Bouchaud, J. P.; Cipelletti, L.; El Masri, D.; L'Hôte, D.; Ladieu, F.; Pierno, M. *Science* **2005**, *310*, 1797–1800.

(57) Andreozzi, L.; Faetti, M.; Giordano, M. *J. Non-Cryst. Solids* **2006**, *352*, 3829–3834.

(58) Cicerone, M. T.; Blackburn, F. R.; Ediger, M. D. *J. Chem. Phys.* **1995**, *102*, 471–479. Heuberger, G.; Sillescu, H. *J. Phys. Chem.* **1996**, *100*, 15255–15260. Corti, H. R.; Frank, A.;

Marconi, M. C. *J. Phys. Chem. B* **2008**, *112*, 12899–12906. Rajian, J. R.; Quitevis, E. L. *J. Chem. Phys.* **2007**, *126*, 224506. Voronel, A.; Veliyulin, E.; Machavariani, V. S.; Kisliuk, A.; Quitmann, D. *Phys. Rev. Lett.* **1998**, *80*, 2630–2633. Ye, J. Y.; Hattori, T.; Nakatsuka, H. *Phys. Rev. B* **1997**, *56*, 5286–5296. Hooker, J. C.; Torkelson, J. M. *Macromolecules* **1995**, *28*, 7683–7692.

(59) Berthier, L. *Phys. Rev. E* **2004**, *69*, 020201(R). Bordat, P.; Affouard, F.; Descamps, M.; Müller-Plathe, F. *J. Phys.: Condens. Matter* **2003**, *15*, 5397–5407. Lombardo, T. G.; Debenedetti, P. G.; Stillinger, F. H. *J. Chem. Phys.* **2006**, *125*, 174507. Kumar, S. K.; Szamel, G.; Douglas, J. F. *J. Chem. Phys.* **2006**, *124*, 214501. Chaudhuri, P.; Berthier, L.; Kob, W. *Phys. Rev. Lett.* **2007**, *99*, 060604.

(60) Andreozzi, L.; Faetti, M.; Giordano, M.; Palazzuoli, D.; Galli, G. *Mol. Cryst. Liq. Cryst.* **2004**, *411*, 515–523. Andreozzi, L.; Faetti, M.; Zulli, F.; Giordano, M.; Galli, G. In *Highlights in the quantum theory of condensed matter*; Beltram, F., Ed. Edizioni della Normale: Pisa, 2005; Quaderni, vol. 1, p 81–101.

(61) Andreozzi, L.; Faetti, M.; Giordano, M.; Palazzuoli, D.; Laus, M.; Galli G. *Macromol. Chem. Phys.* **2002**, *203*, 1636–1642.

(62) Andreozzi, L.; Giordano, M.; Leporini, D. In *Structure and Transport Properties in Organized Materials*; Chiellini, E., Giordano, M., Leporini, D., Eds.; World Scientific: Singapore, 1997; p 241.

(63) Galli, G.; Szanka, I.; Andreozzi, L.; Autiero, C.; Faetti, M.; Giordano, M.; Zulli, F. *Macromol. Symp.* **2006**, *245–246*, 463–469.

(64) Andreozzi, L.; Faetti, M.; Giordano, M. *J. Phys.: Condens. Matter* **2006**, *18*, 931–940;

(65) Guenza, M. *Phys. Rev. Lett.* **2002**, *88*, 025901. Guenza, M. *J. Chem. Phys.* **2003**, *119*, 7568–7578.

(66) Andreozzi, L.; Autiero, C.; Faetti, M.; Giordano, M.; Zulli, F.; Galli, G.; *Mol. Cryst. Liquid Cryst.* **2006**, *450*, 163–171.

(67) Fetters, L. J.; Lohse, D. J.; Richter, D.; Witten, T. A.; Zirkel, A. *Macromolecules* **1994**, *27*, 4639–4647.

(68) Zulli, F. PhD Thesis, University of Pisa, 2008; Zulli, F.; Giordano, M.; Andreozzi, L. *Rheol. Acta* **2015**, *54*, 185–205; and references therein.

(69) McCrum, N. G.; Read, B. E.; Williams, G. *Anelastic and Dielectric Effects in Polymeric Solids*; Dover Publications: New York, 1991. Hayakawa, T.; Adachi, K. *Polym. J.* **2000**, *32*, 845–848.